Construction of π-Stacked Supramolecular Framework Using Triphenylene-cored Metallo-organic Cage

Zhilong Jiang,‡[a] Jun Wang,‡[a] Mingzhao Chen,*[a] Chaolong Tang,[c] He Zhao,[b] Qiangqiang Dong,[b] Weidong Yu,[b] Zhiyuan Jiang,[b] Bangtang Chen,[a] Xiaorui Li,[b] Die Liu,[b] Liao-Yuan Yao,[d] Hui Liu,[b] Tingzheng Xie,[a] Tun Wu,[a] Jie Yuan,[e] Kun Wang,[c] Yiming Li,*[b] Pingshan Wang*[a,b]

Table of Contents

1. Materials and Methods

1.1 General

All starting materials were purchased from Aldrich, Alfa Aesar and used without further purification. Compound **2** (2,3,6,7,10,11-hexabromotriphenylene) and compound **3** (3'-boronatopenyl[2,2':6',2"]terpyridine) were synthesized according to the reported methods[S1-2]. Column chromatography was conducted by using basic Al_2O_3 (sinopharm chemical reagents co., Ltd, 200-300 mesh) or SiO_2 (Qingdao Haiyang Chemical co., Ltd, 200-300 mesh).

1.2 Characterization Methods

The ^1H NMR and ^{13}C NMR spectra were recorded on a Bruker Avance 400-MHz and 500-MHz NMR spectrometer in $CDCl_3$, DMF-d7, and CD_3CN with TMS as the internal standard. Transmission Electron Microscopy (TEM) was obtained on JEOL 2010. ESI mass spectrometry (ESI-MS) and traveling wave ion mobility (TWIM) experiments were conducted on a Waters Synapt HDMS G2 instrument with a LockSpray ESI source. Data were collected and analyzed by using MassLynx 4.1 and DriftScope 2.4 (Waters). Scanning Tunneling Microscope (STM): The sample was dissolved in DMF or CH_3CN at a concentration of 5.0 mg/mL. Solution (5uL) was dropped on HOPG surface. After 30 seconds, the surface was washed slightly with water for three times and totally dried in air. The STM images were taken with a PicoPlus SPM system with a PicoScan 3000 Controller. The obtained STM images were processed by WSxM software.[3] Atomic Force Microscop (AFM) was used to make markers on the surface of the sample with nanoshaving technique. The size of the markers is 10μm×10μm and the distances between two closest markers are 30μm. The loading forces used are 6μN and shaving speed is around 5μm/s. SCXRD analysis was performed on a Bruker APEX3 diffractometer. The structure was solved with the ShelXT structure solution program using intrinsic phasing and refined with the ShelXL refinement package using least squares minimization. The Solvent Mask routine of the OLEX2 software was implemented to remove the contributions of DMF solvent and ethyl acetate solvent to observed structure factors. “SIMU” directive and “DELU” directive was used to constrain C74~C75, C80~C84, C100~C104 and C178~C182. Thermogravimetric data (TG) was collected with a Rigaku TGA-8120 instrument at a heating rate of 10 ºC/min in nitrogen gas. The cumulative apparent surface areas for N_2 were calculated on a Micro ASAP 2020 using a Brunauer–Emmett–Teller (BET) model range from 0.01 to 0.1 bar for **[$Zn_{12}L_4$]**.

2. Synthesis of the Ligand L and complex [$Zn_{12}L_4$]

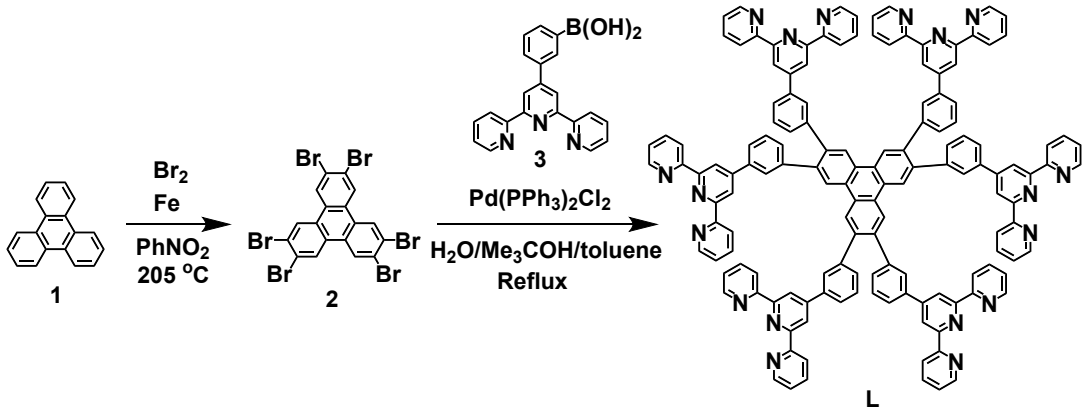

Scheme S1: Synthesis of Ligand **L.**

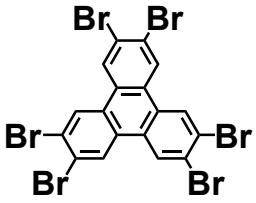

Compound 2: This compound was synthesized according to a published procedure[S1]. By mixing 1.00 g (4.38 mmol) of triphenylene **1** and 90 mg of Fe dissolved in 20 ml of nitrobenzene, 3.15 g (39.42 mmol) of Br_2 was added dropwise slowly at room temperature, stirred at 205° C for 3 h. After cooling to the room temperature, 50 ml of ether was added, which was filtered and washed with ether (3×30 mL) and acetone (3×10 mL), generated the compound **2**: 2.80 g, 91.2%.

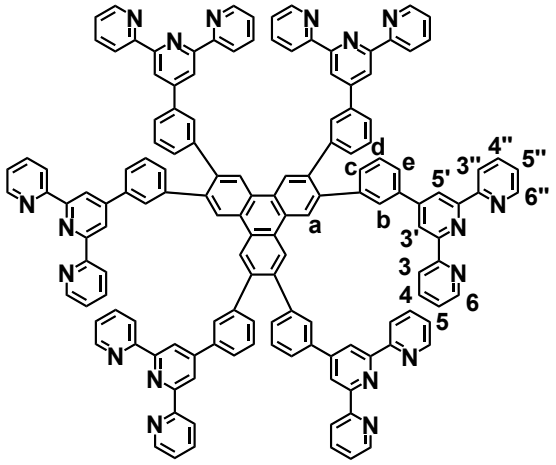

Ligand L: Compound **2** (200.2 mg, 285.6 μmol) and 3'-boronatopenyl[2,2':6',2'']terpyridine **3** (786.3 mg, 2.23 mmol) was added to a 250 mL flask, then H_2O:Me_3COH:toluene (200 mL, V:V:V, 3:1:3) and Na_2CO_3 (544.9 mg, 5.14 mmol) in 3.9 mL of water was added, The system

was degassed for 10 min, and $Pd(PPh_3)_2Cl_2$ (72.07 mg, 102.8 μmol) as the catalyst was added. The mixture was stirred at 90 °C under nitrogen for 6 d, after cooled to ambient temperature, purified through recrystallization of MeOH/$CHCl_3$, a white solid was generated: 447.0 mg, 62 %. ^{1}H NMR (500 MHz, $CDCl_3$, ppm) δ8.90 (s, 6H, Ph-H^a), 8.59-8.58 (d, 12H, tpy-$H^{6,6'}$), 8.53-8.51 (m, 24H, tpy-$H^{3',5'}$, tpy-$H^{3,3''}$), 7.93 (s, 6H, Ph-H^b), 7.80-7.76 (m, 18H, tpy-$H^{4,4''}$, Ph-H^c), 7.53-7.51 (d, 6H, J=10 Hz, Ph-H^e), 7.48-7.55 (m, 6H, Ph-H^d), 7.24-7.22 (t, 12H, tpy-$H^{5,5''}$). ^{13}C NMR (101 MHz, $CDCl_3$) δ 156.14, 155.77, 150.14, 149.02, 141.92, 139.57, 138.40, 136.59, 131.01, 129.21, 129.01, 128.79, 126.03, 125.65, 123.60, 121.21, 119.08. ESI-MS (2071.7629 calcd. for $C_{144}H_{90}N_{18}$): m/z 2073.7957 $(M + H^+)^+$ (calcd m/z: 2073.7751).

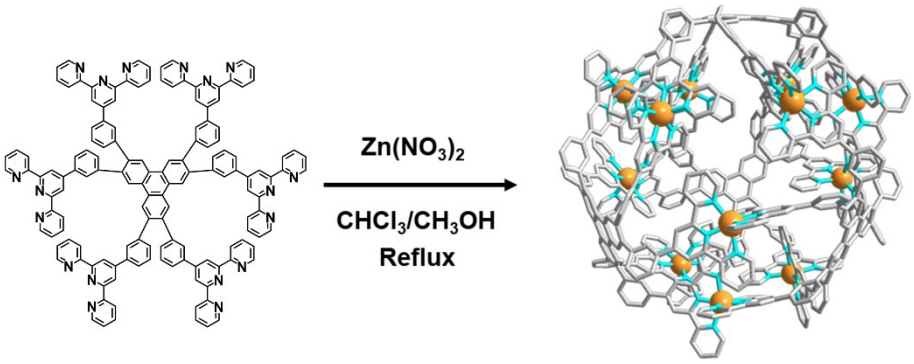

Scheme S2: Synthesis of metallo-organic cage **[$Zn_{12}L_4$]**.

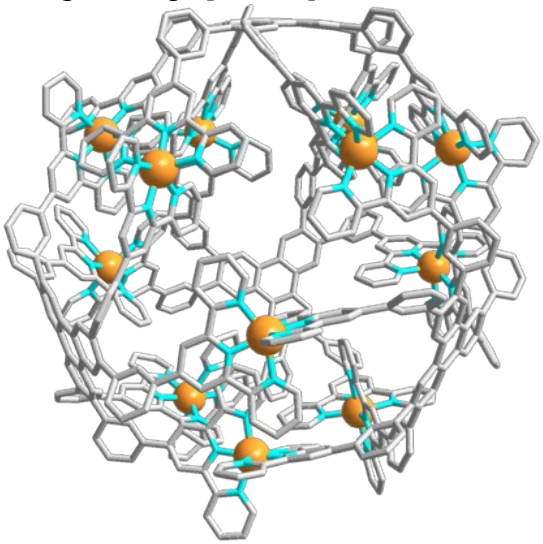

Complex [$Zn_{12}L_4$]: Ligand **L** (23.0 mg, 11.1 μmol) and $Zn(NO_3)_2·6H_2O$ (10.4 mg, 34.9 μmol) was added in a 50 ml flask, then a solvent mixture of MeOH and $CHCl_3$ (20 ml, V:V, 1:2) was added. The mixture was refluxed for 12 h, after cooled to ambient temperature, excess NH_4PF_6 in MeOH was added to get a white precipitate, which was filtered and washed with MeOH to generate a faint yellow solid: 33.8 mg, 97%. ^{1}H NMR (500 MHz, DMF-d7/CD_3CN, ppm) δ9.33 (s, 24H, B-tpy-$H^{3',5'}$), 9.25 (s, 12H, B-Ph-H^a), 9.14 (s, 12H, B-Ph-H^b), 8.81 (s, 12H, A-Ph-H^a), 8.62-8.60 (m, 36H, B-tpy-$H^{3,3''}$, B-Ph-H^e), 8.24-8.22 (m, 24H, A-Ph-H^c, A-Ph-H^e), 8.19-8.16 (d, 24H, J=15 Hz, A-tpy-$H^{3,3''}$), 8.07 (s,

24H, A-tpy-$H^{3',5''}$), 7.99-7.97 (m, 12H, A-Ph-H^{d}), 7.81-7.77 (m, 24H, B-tpy-$H^{4,4''}$), 7.75-7.71 (m, 24H, A-tpy-$H^{4,4''}$), 7.65-7.62 (m, 24H, A-Ph-H^{b}, B-Ph-H^{d}), 7.60-7.59 (d, 24H, J=5 Hz, A- tpy-$H^{6,6''}$), 7.49-7.48 (d, 24H, J=5 Hz, B- tpy-$H^{6,6''}$), 7.42-7.40 (d, 12H, J=10 Hz, B-Ph-H^{c}), 7.14-7.12 (m, 24H, A-tpy-$H^{5,5''}$), 7.02-6.99 (m, 24H, B-tpy-$H^{5,5''}$). ESI-MS (12553.4203 calcd. for $C_{576}H_{360}F_{144}N_{72}P_{24}Zn_{12}$ with PF_6^-): m/z 2364.9014 $(M-5PF_6^-)^{5+}$ (calcd m/z: 2365.7041), 1946.7607 $(M-6PF_6^-)^{6+}$ (calcd m/z: 1947.2767), 1648.0940 $(M-7PF_6^-)^{7+}$ (calcd m/z: 1648.3737), 1424.1114 $(M-8PF_6^-)^{8+}$ (calcd m/z: 1424.2075), 1249.3151 $(M-9PF_6^-)^{9+}$ (calcd m/z: 1249.8545), 1110.1103 $(M-10PF_6^-)^{10+}$ (calcd m/z: 1110.3820), 996.0016 $(M-11PF_6^-)^{11+}$ (calcd m/z: 996.2500).

3. NMR spectra of ligand L and complex [$Zn_{12}L_4$]

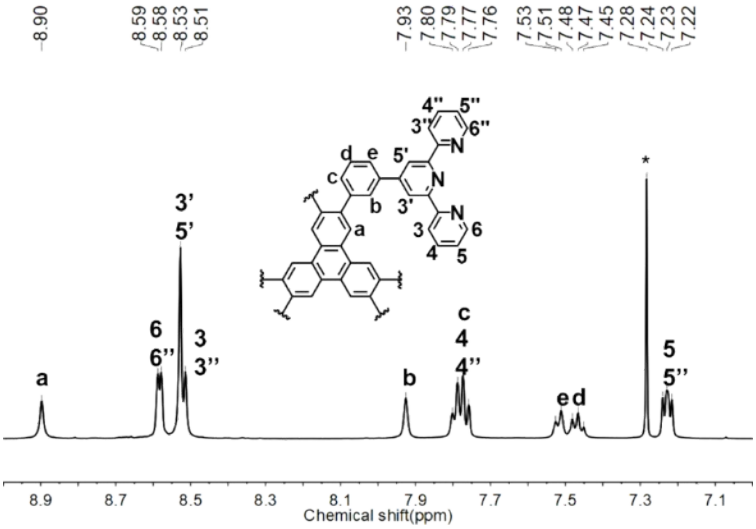

Figure S1. ^{1}H NMR spectrum (400 MHz) of ligand **L** in $CDCl_3$.

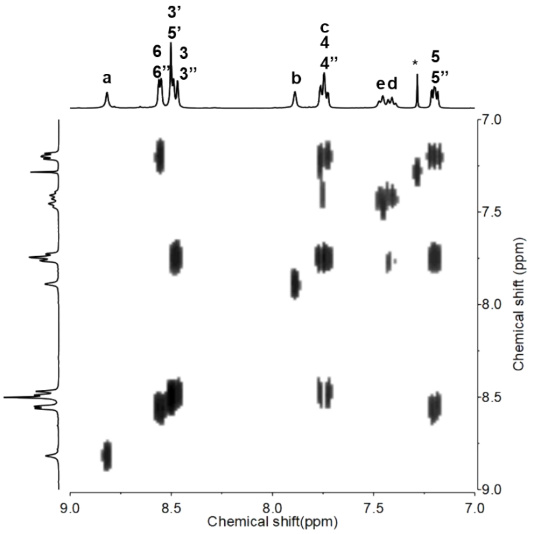

Figure S2. 2D COSY NMR spectrum (400 MHz) of ligand **L** in $CDCl_3$.

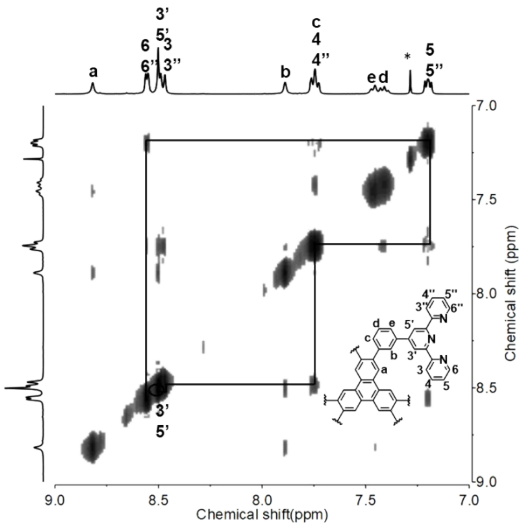

Figure S3. 2D NOESY NMR spectrum (400 MHz) of ligand **L** in $CDCl_3$.

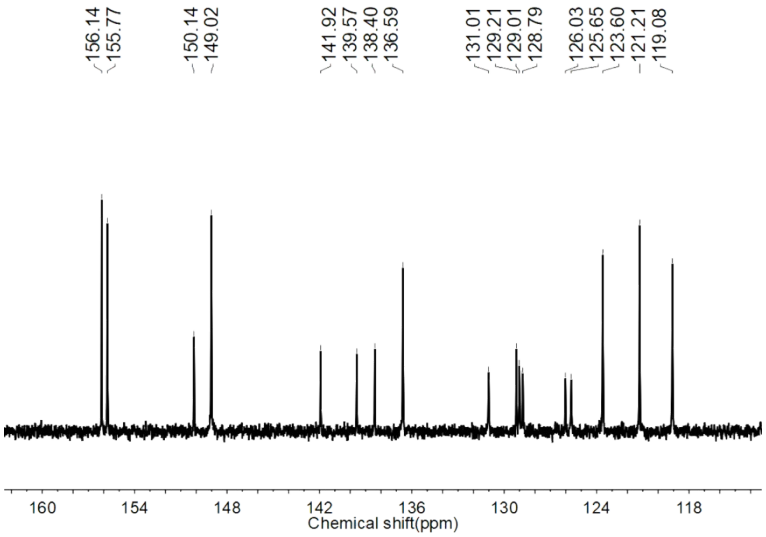

Figure S4. ^{13}C NMR spectrum (101 MHz) of **L** in $CDCl_3$.

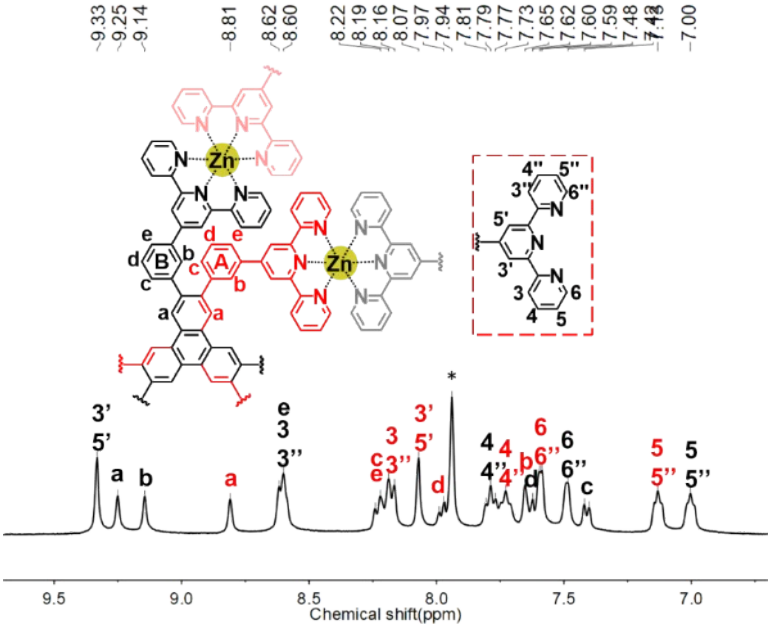

Figure S5. ^{1}H NMR spectrum (400 MHz) of **[$Zn_{12}L_4$]** in CD_3CN/DMF-d_7 (v/v, 1:9).

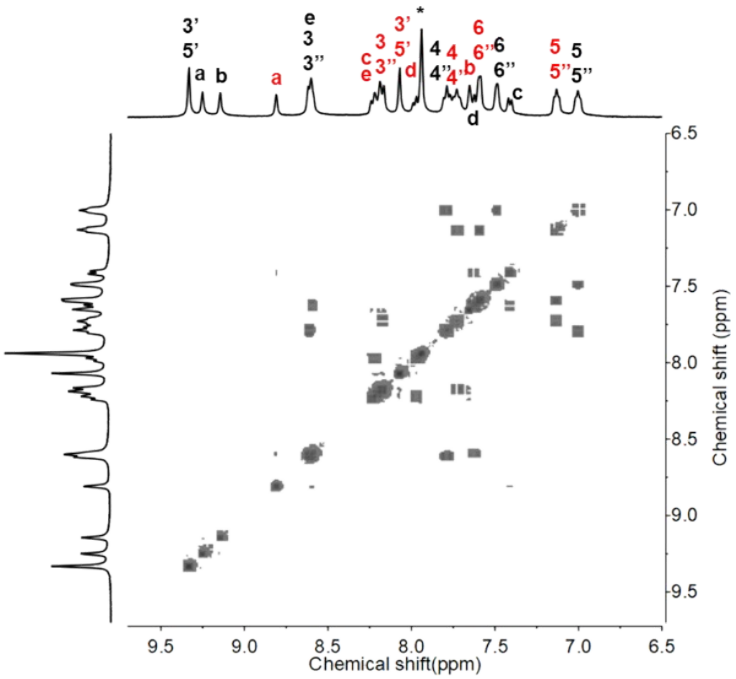

Figure S6. 2D COSY NMR spectrum (400 MHz) of **[$Zn_{12}L_4$]** in CD_3CN/DMF-d_7 (v/v, 1:9).

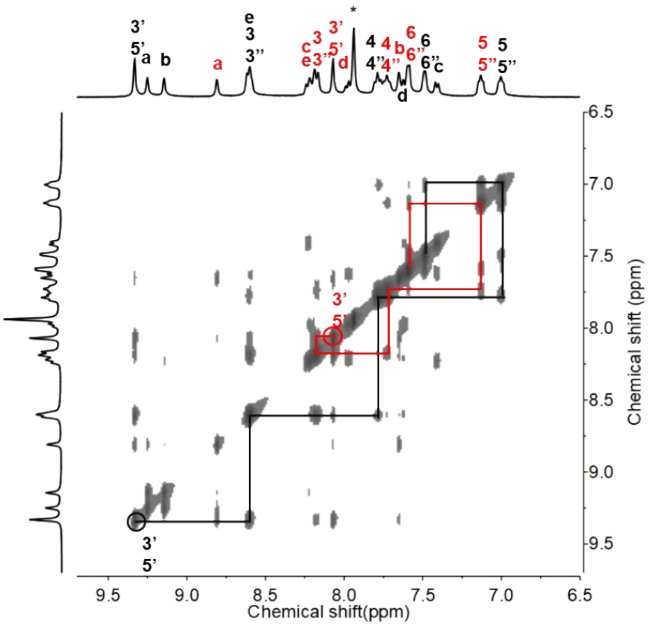

Figure S7. 2D NOESY spectrum (400 MHz) of **[$Zn_{12}L_4$]** in CD_3CN/DMF-d_7 (v/v, 1:9).

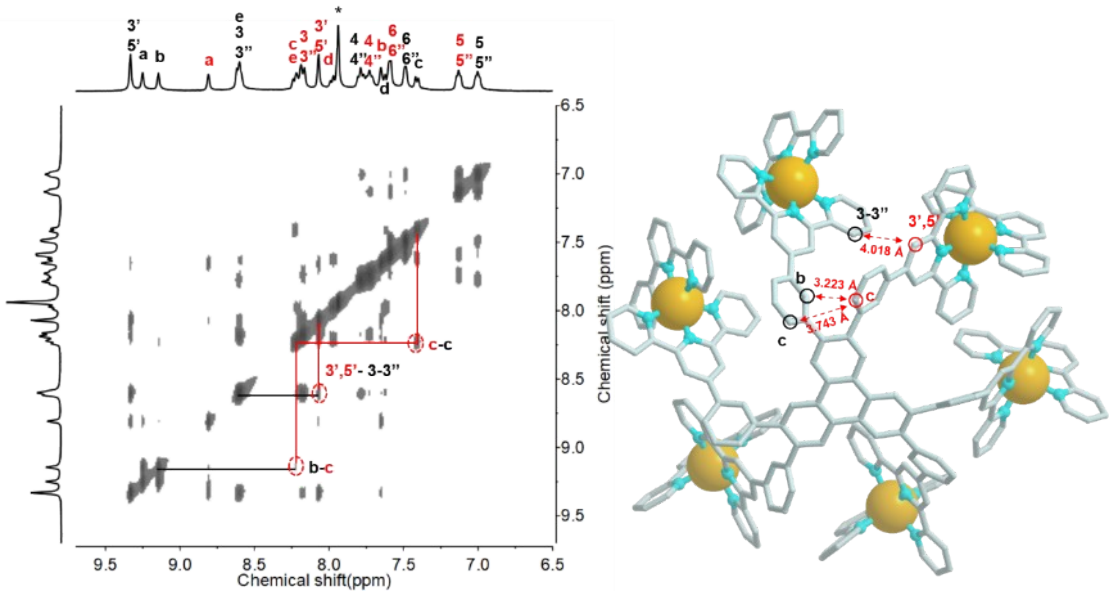

Figure S8. 2D NOESY spectrum (400 MHz) of **[$Zn_{12}L_4$]** in CD_3CN/DMF-d_7 (v/v, 1:9).

From the crystal structure, protons A-H^b, A-tpy-$H^{3,3''}$, A-H^c are only 3.223 Å, 3.743 Å, and 4.018 Å away from protons B-H^c, B-tpy-$H^{3',5'}$, and B-H^c, respectively. Simultaneously, the 2D NOESY spectrum of supramolecular cage **[$Zn_{12}L_4$]** clearly shows spatial correlation between A-H^b, A-tpy-$H^{3,3''}$, A-H^c with B-H^c, B-tpy-$H^{3',5'}$, B-H^c, respectively. The correlation between the two kinds of tpy units proves that they belong to the same molecule.

Based on the crystal structure of **[$Zn_{12}L_4$]**, its symmetry is reduced due to molecular distortion, resulting in two types of terpyridine (denoted by different colors). Based on the triphenylene plane, the red terpyridine part (^{A}-tpy) has a greater degree of rotation than the green terpyridine part (^{B}-tpy). The delocalized π electron of triphenylene might generate a ring current and induce a magnetic field under the external magnetic field (Figure S9). In addition, the distance between the benzene ring center of ^{A}-tpy-$H^{3',5'}$ and ^{B}-tpy-$H^{3',5'}$ and triphenylene center is different (Figure S10). We speculate that ^{A}-tpy-$H^{3',5'}$ proton is in the high de-shielding regions and ^{B}-tpy-$H^{3',5'}$ proton in the low de-shielding regions. Under this de-shielding force, the chemical shift of ^{A}- tpy-$H^{3',5'}$ proton is located in the low field and the ^{B}-tpy-$H^{3',5'}$ proton is in the high field.

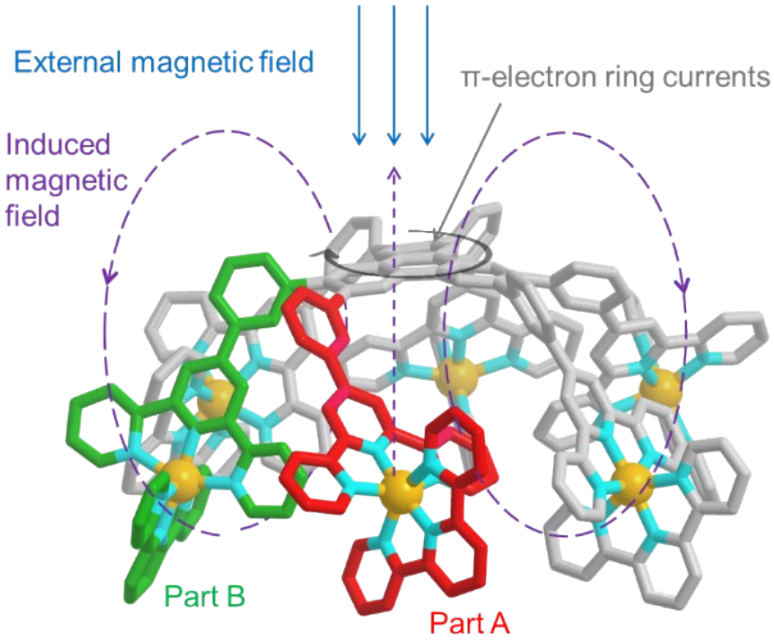

Figure S9. Summary diagram of shielding effect.

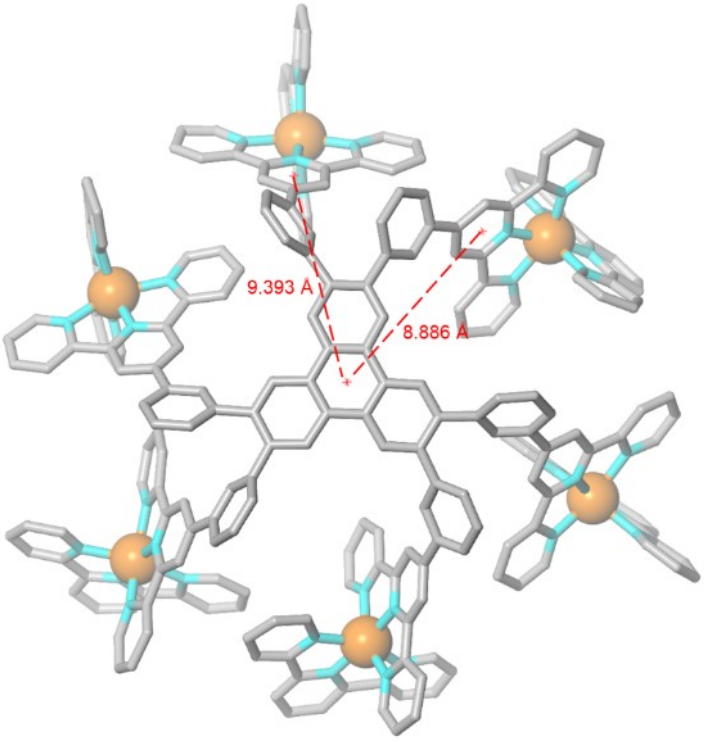

Figure S10. Local structure diagram of supramolecule **[$Zn_{12}L_4$].**

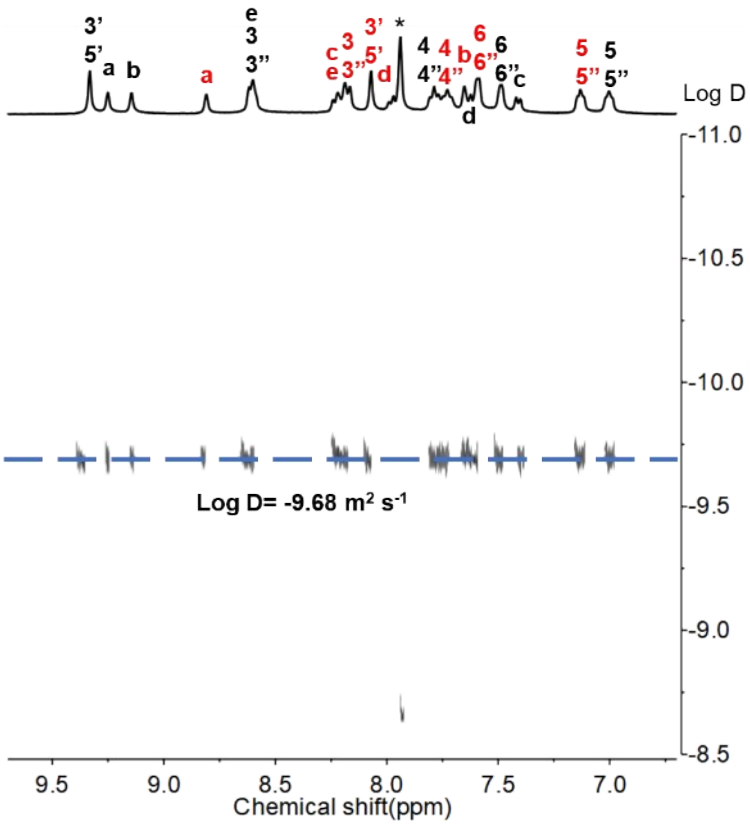

Figure S11. 2D DOSY spectrum (500 MHz) of **[$Zn_{12}L_4$]** in CD_3CN/DMF-d_7 (v/v, 1:9).

The metallo-organic cage's hydrodynamic radius was estimated according to the Stokes-Einstein Equation,

$$D = \frac{kT}{6\pi\mu \mathrm{rH}}$$

where D is the diffusion constant,

k is the Boltzmann's constant,

T is the temperature,

μ is the viscosity of solvents,

r_H is the hydrodynamic radius

$D = 2.09\times10^{-10}$ m^2 s^{-1}

$k = 1.38\times10^{-23}$ N m K^{-1}

$T = 298$ K

$\mu = 7.48\times10^{-4}$ N m^{-2} s (CD_3CN/DMF-d_7 (1:9, v/v))

$$\mathrm{rH} = \frac{kT}{6\pi\mu D} = 1.4\times10{-}9\ m\ =\ 1.4\ nm$$

The 2D DOSY spectrum of **[$Zn_{12}L_4$]** showed a narrow band at log D= -9.68 m^2 s^{-1} corresponding to the ^{1}H NMR spectrum, indicating that only solely composition exists in the solvent. The radius of the supramolecular cage **[$Zn_{12}L_4$]** was calculated as 1.4 nm based on Stokes-Einstein Equation, which agreed well with the diameter measured in single crystal structure.

4. ESI-MS spectra data of ligand L and $[Zn_{12}L_4]$

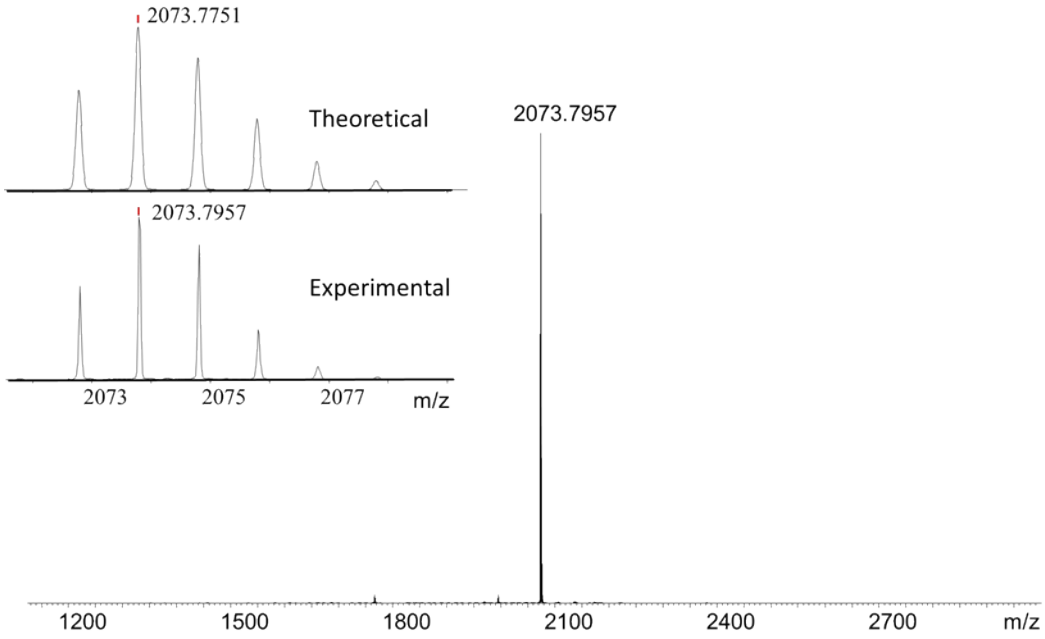

Figure S12. ESI-MS spectrum of ligand **L**.

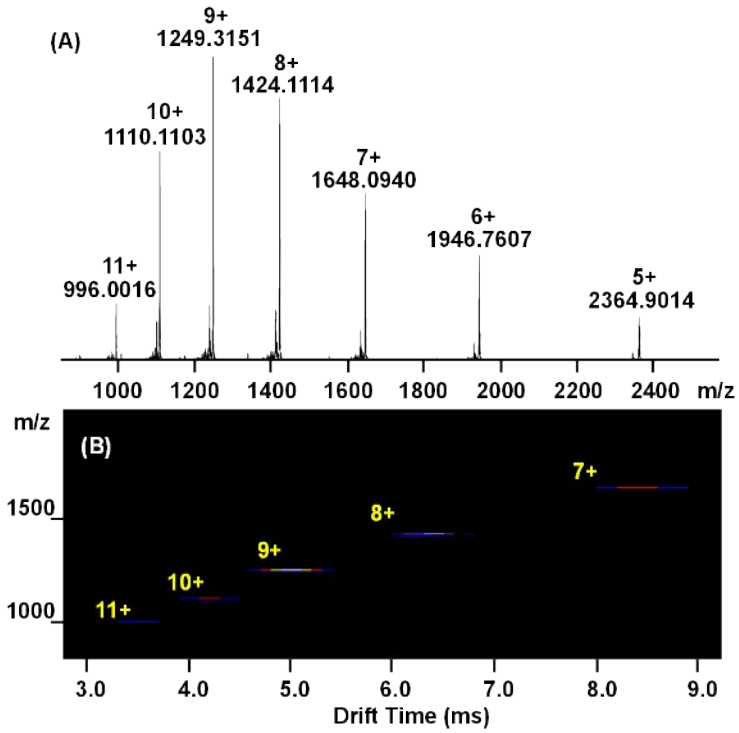

Figure S13. (A) ESI-MS spectrum and (B) TWIM-MS plots of **$[Zn_{12}L_4]$** (PF_6^- as counterion).

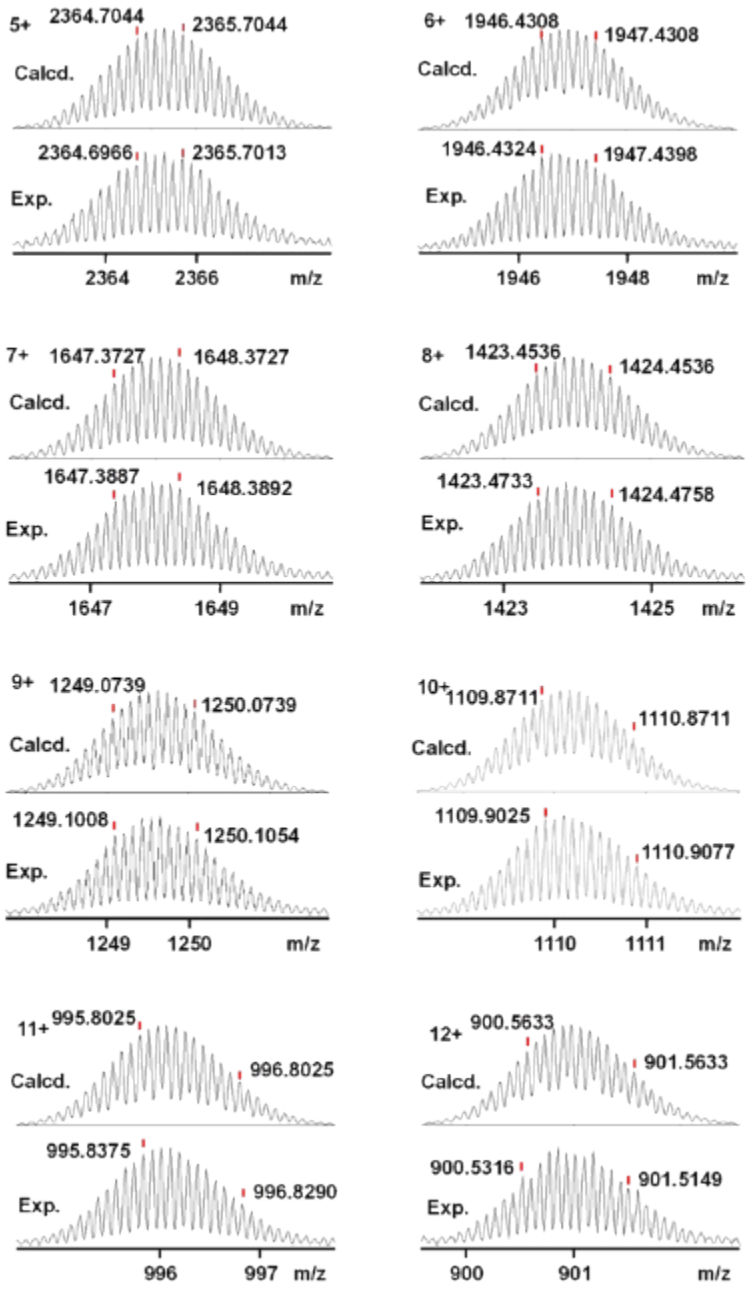

Figure S14. Isotope patterns for the different charge states observed from **[$Zn_{12}L_4$]** (PF_6^- as counterion).

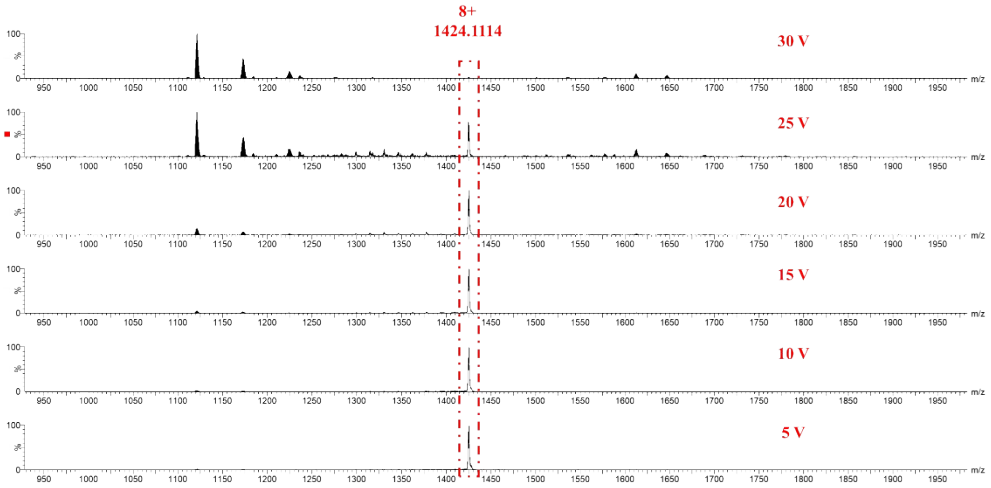

Figure S15. gMS^2 of **[$Zn_{12}L_4$]** at m/z 1424.1114 (8+ ions) with different collision energies.

5. The thermal stability of [$Zn_{12}L_4$]

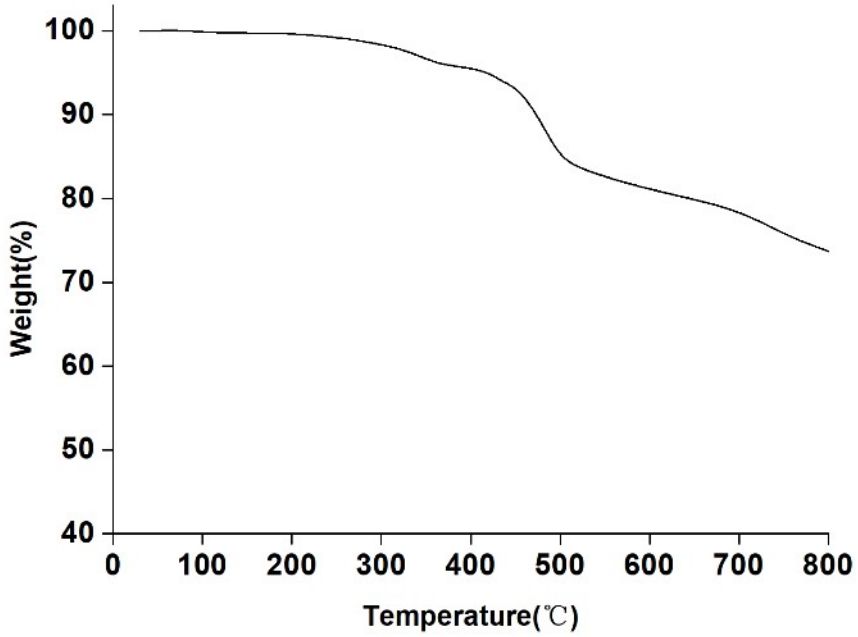

Figure S16. TG data of **[$Zn_{12}L_4$]** under N_2 atmosphere.

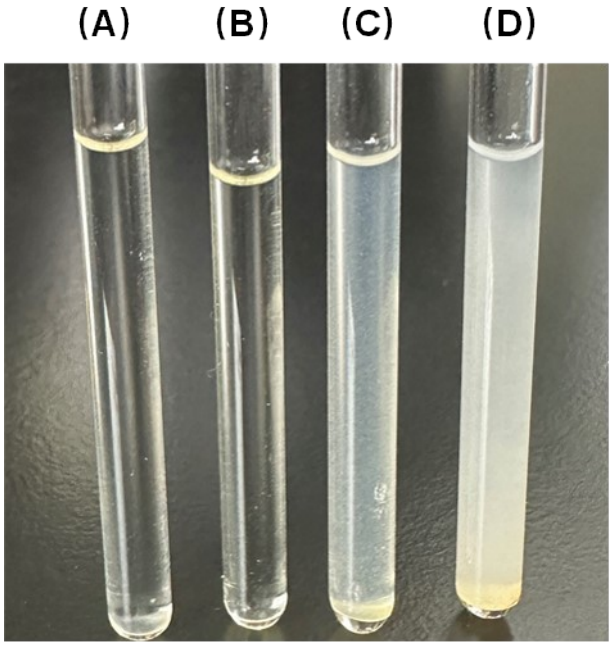

Figure S17. Solution of **[$Zn_{12}L_4$]** solid after heated at (A) 100℃, (B) 150℃, (C) 200℃, and (D) 250℃ for 20 minutes (in CD_3CN/DMF-d_7, v/v, 1:4).

[$Zn_{12}L_4$] solid exhibited good stability below 150℃, when the temperature reaches 200℃, **[$Zn_{12}L_4$]** solid shows instability and partial insolubility (in CD_3CN/DMF-d_7, v/v, 1:4), it completely dissociates at a temperature of 250℃.

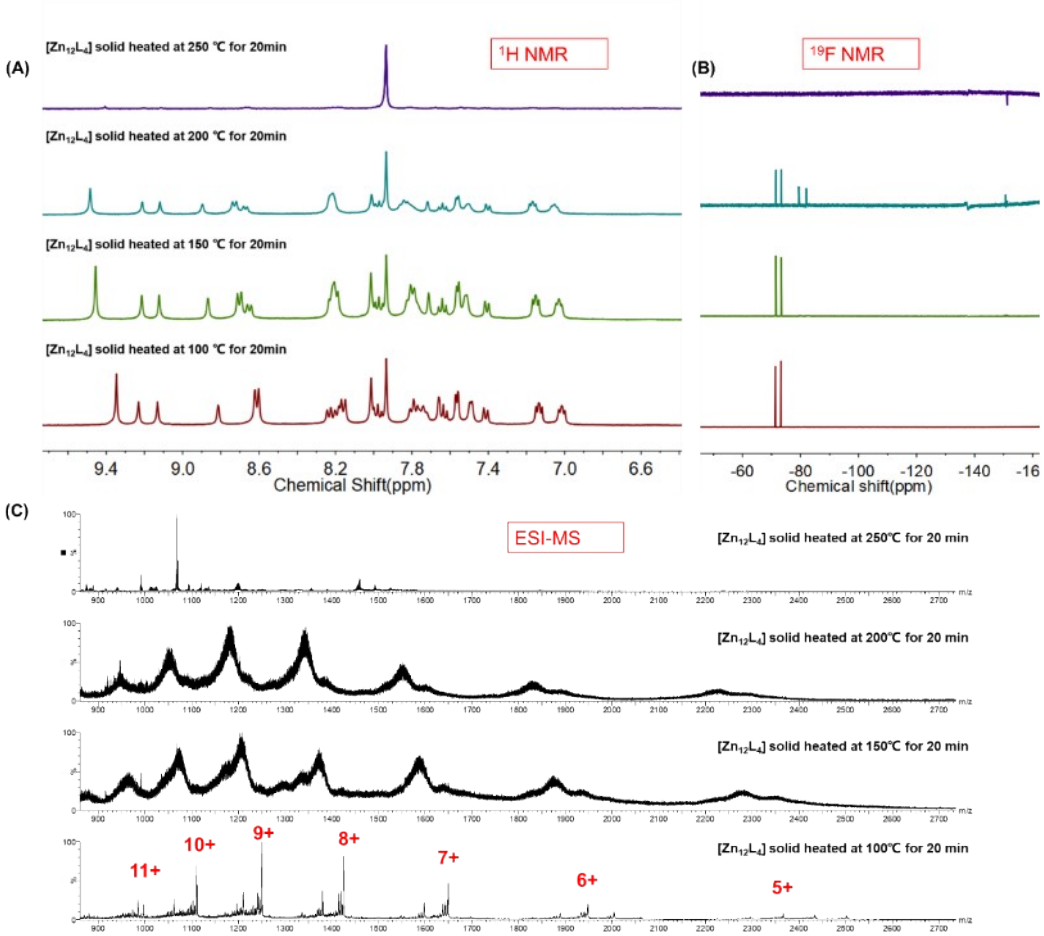

Figure S18. (A) ^{1}H NMR spectra, (B) ^{19}F NMR spectra (dissolved in CD_3CN/DMF-d_7, v/v, 1:4), and (C) ESI-MS of **[$Zn_{12}L_4$]** solid after heated at 100℃, 150℃, 200℃, and 250℃ for 20 minutes. ^{1}H NMR of **[$Zn_{12}L_4$]** after solid heated at 100℃, 150℃, 200℃, and 250℃ showed that **[$Zn_{12}L_4$]** solid exhibits good stability below 200℃, it completely dissociates at a temperature of 250℃. ESI-MS data indicated that **[$Zn_{12}L_4$]** after solid heated at 100℃ remains stable and unchanged, and the framework remains stable at 150 and 200℃, but a series of F in PF_6 counterions were dissociated, which led to a broadening of the ESI-MS spectrum and a decrease in molecular weight. ^{19}F NMR also confirmed the dissociation of F, which showed that some other F signals appeared at temperatures of 150 and 200°C.

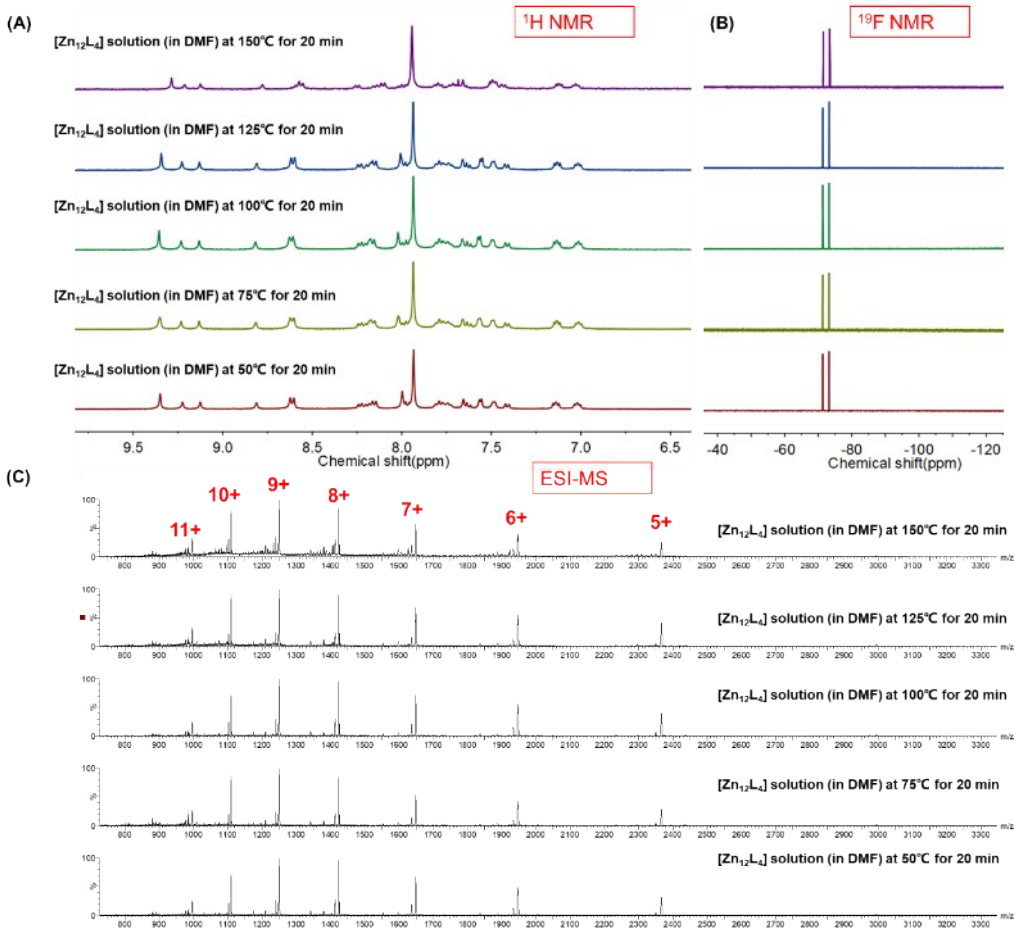

Figure S19. (A) ^{1}H NMR spectra, (B) ^{19}F NMR spectra (dissolved in CD_3CN/DMF-d_7, v/v, 1:4), and (C) ESI-MS of **[$Zn_{12}L_4$]** solution after heated at 50℃, 75℃, 100℃, 125℃, and 150℃ for 20 minutes. After the DMF solution of **[$Zn_{12}L_4$]** was heated at 50℃, 75℃, 100℃, 125℃, and 150℃, ^{1}H NMR, ^{19}F NMR and ESI-MS showed that **[$Zn_{12}L_4$]** solution exhibits good stability and remains unchanged at above temperatures

6. The host-guest chemistry of [$Zn_{12}L_4$]

From the crystal data, supramolecule **[$Zn_{12}L_4$]** shows an incompletely closed cage structure. Since the side length of the triangular face is about 1.7 nm, such cage has windows with a diameter around 0.9 nm and an inner cavity about 2143 Å^3 for encapsulation of guest molecules. On account of the strong affinity between triphenylene and fullerenes through π-π stacking, C_{60} was selected to investigate the host-guest chemistry of the supramolecular cage**.** The encapsulation of fullerene occurs upon mixing C_{60} simultaneously with the metallo-organic cage **[$Zn_{12}L_4$]** in DMF/CH_3CN, followed by heating at 90 °C for 24 h.

The ESI-MS revealed a series of continuous signal peaks of host-guest molecule $C_{60} \subset$ **[$Zn_{12}L_4$]**, indicating the successful encapsulation of the guest molecule C_{60} in the supramolecular cage **[$Zn_{12}L_4$]**. Furthermore, gradient tandem-mass spectrometry (gMS^2) was used to test the stability of the host-guest system of $C_{60} \subset$ **[$Zn_{12}L_4$]**. As shown in Figure S20, $C_{60} \subset$ **[$Zn_{12}L_4$]** displayed good

stability under a voltage of 24 V in the ESI-MS collision induced dissociation experiments, which suggested that the guest molecule C_{60} has a strong affinity with the triphenylene-based cage.

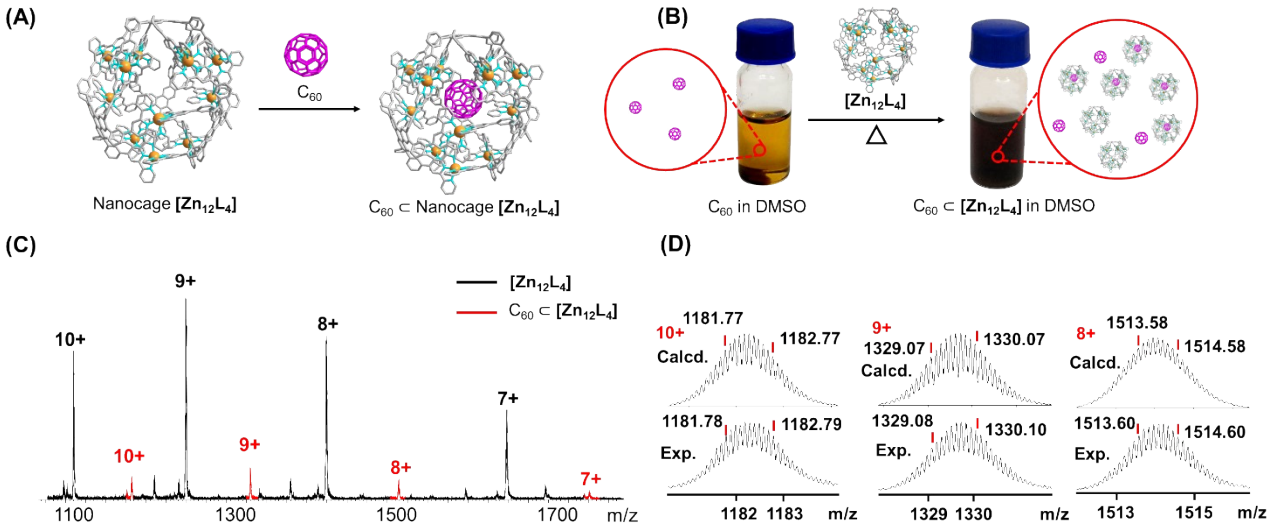

Figure S20. (A) Formation of $C_{60} \subset$ **[$Zn_{12}L_4$].** (B) Photographs show C_{60} dissolved in DMSO and $C_{60} \subset$ **[$Zn_{12}L_4$]** dissolved in DMSO. (C) ESI-MS spectrum for the reaction mixture containing $C_{60} \subset$ **[$Zn_{12}L_4$]** (red peaks) and empty **[$Zn_{12}L_4$]** (black peaks), the low peaks may because the presence of a dynamic equilibrium of one C_{60} within the cavity. (D) Three charge states of $C_{60} \subset$ **[$Zn_{12}L_4$]**, calculated (top) and experimental (bottom).

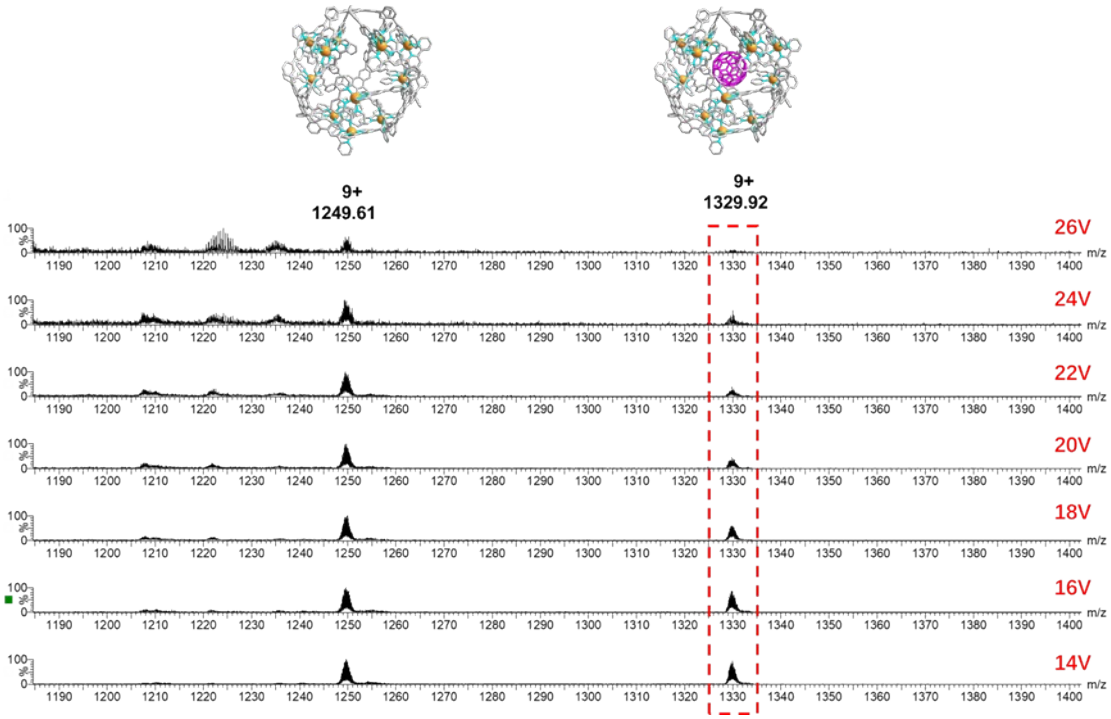

Figure S21. gMS^2 of $C_{60} \subset$ **[$Zn_{12}L_4$]** at m/z 1329.92 with different collision energies.

7. Single-Crystal X-Ray Diffraction of $[Zn_{12}L_4]$

Table S1. Crystal Data and Structure Refinement for **$[Zn_{12}L_4]$**.

CCDC	2109206
Formula	$C_{585}H_{381}N_{75}O_3P_{15}F_{90}Zn_{12}$
Temperature (K)	298(2)
Formula weight (g/mol)	11467.62
Crystal system	trigonal
Space group	P-3
a (Å)	47.503(7)
b (Å)	47.503(7)
c (Å)	29.834(6)
α (°)	90
β (°)	90
γ (°)	120
V, Å^3	58300(20)
Z	2
Calculated density (g cm^{-3})	0.653
μ (mm^{-1})	0.308
2θ (°)	2.158 to 45.924
F (000)	11670.0
Reflections collected	117047
R_{int}	R_{int} = 0.1107
Data/restraints/parameters	41377/100/2343
Goodness-off-fit on F^2	0.999
Final R indices [I>2σ(I)][a]	R_1 = 0.0973, wR_2 = 0.2915
R indices (all data)	R_1 = 0.1250, wR_2 = 0.3217

[a] $R_1 = \Sigma||F_o| - |F_c|| / \Sigma|F_o|$; $wR_2 = [\Sigma [w(F_o^2 - F_c^2)^2] / \Sigma[w(F_o^2)^2]]^{1/2}$

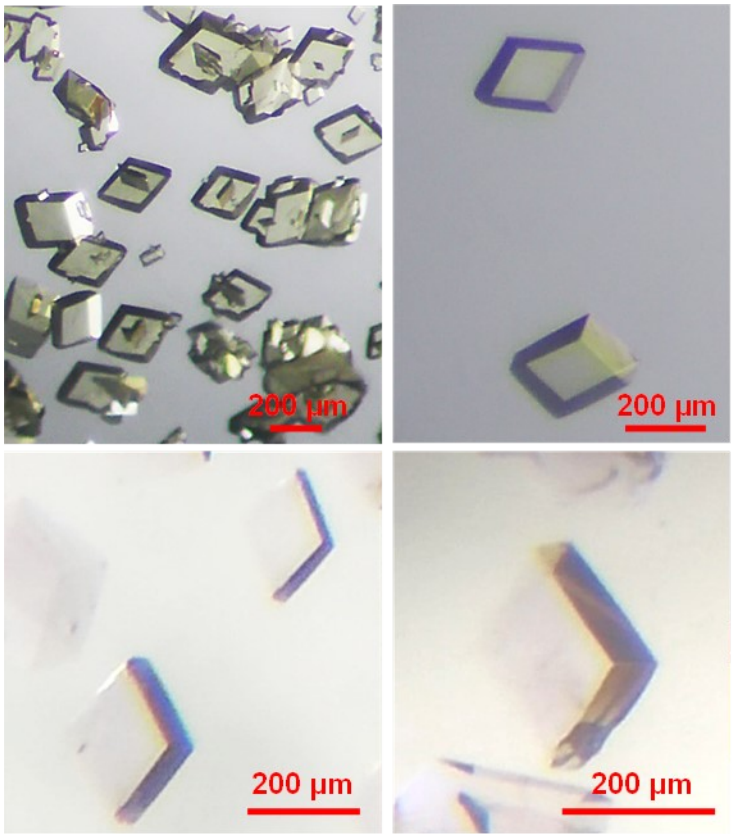

Figure S22. Optical microscope images of **[$Zn_{12}L_4$]** single crystals (achieved through slow evaporation of ethyl acetate into the solution of **[$Zn_{12}L_4$]** in DMF at a constant temperature of 298 K).

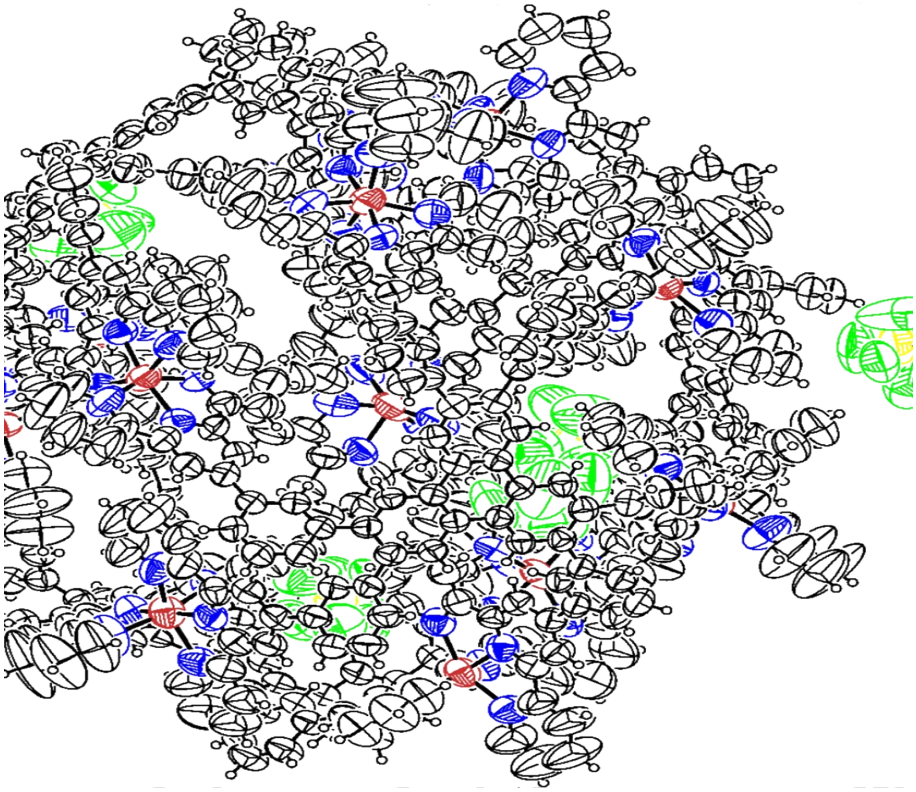

Figure S23. Ortep drawing of the asymmetric unit in the crystal structure of **[$Zn_{12}L_4$]** at 50% probability level.

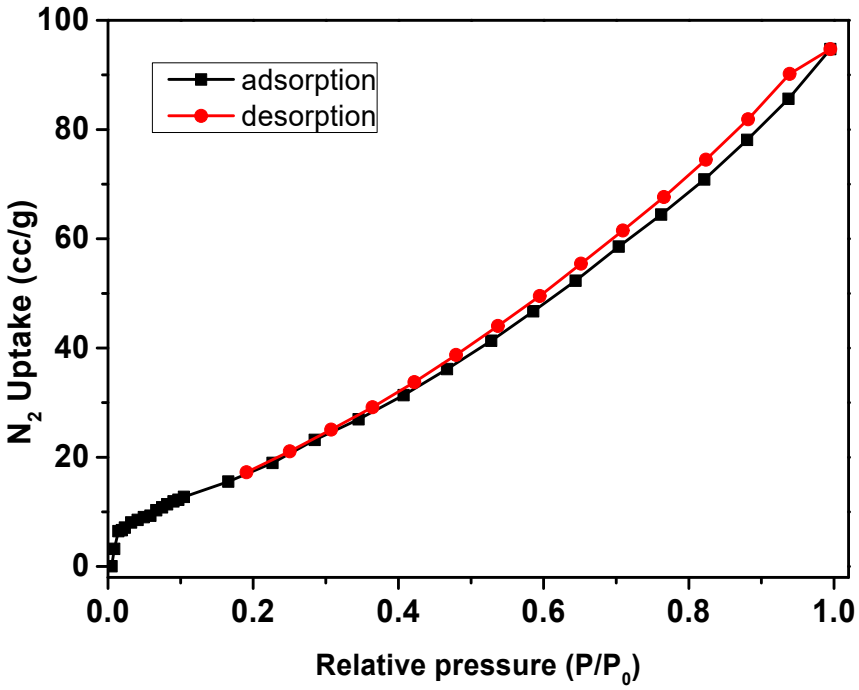

Figure S24. Nitrogen sorption isotherms of **[$Zn_{12}L_4$]** at 77 K.

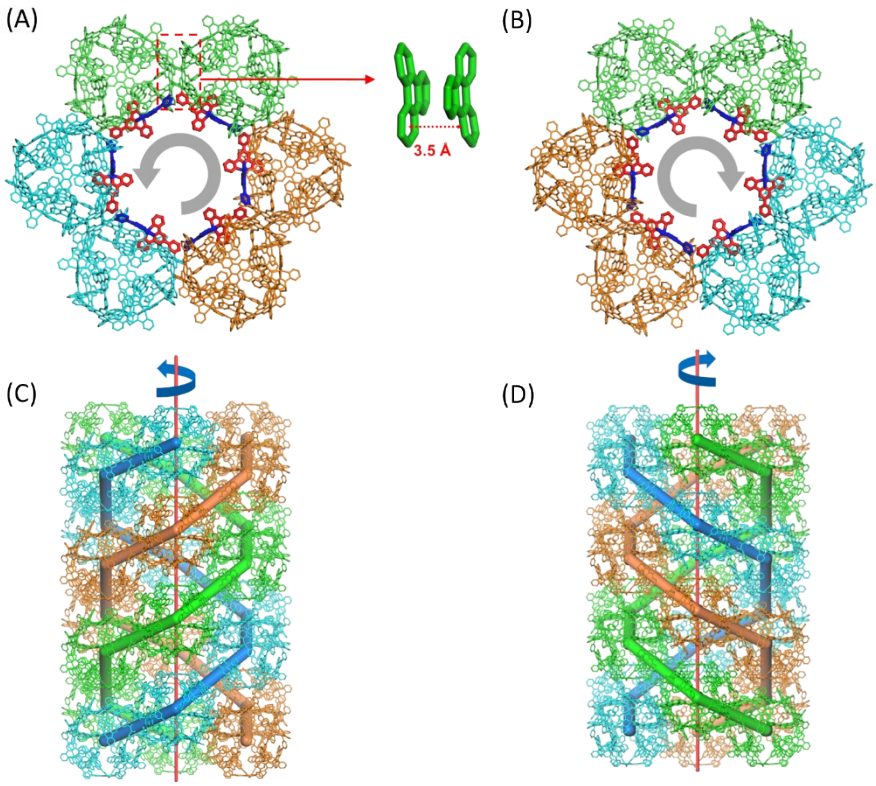

Figure S25. (A, B) Bottom view of the 3D packing for **[$Zn_{12}L_4$]**. (C, D)Triple helically arrangment of the superstructural channel by extracting the cages upwards along the arrow direction in A and B, respectively.

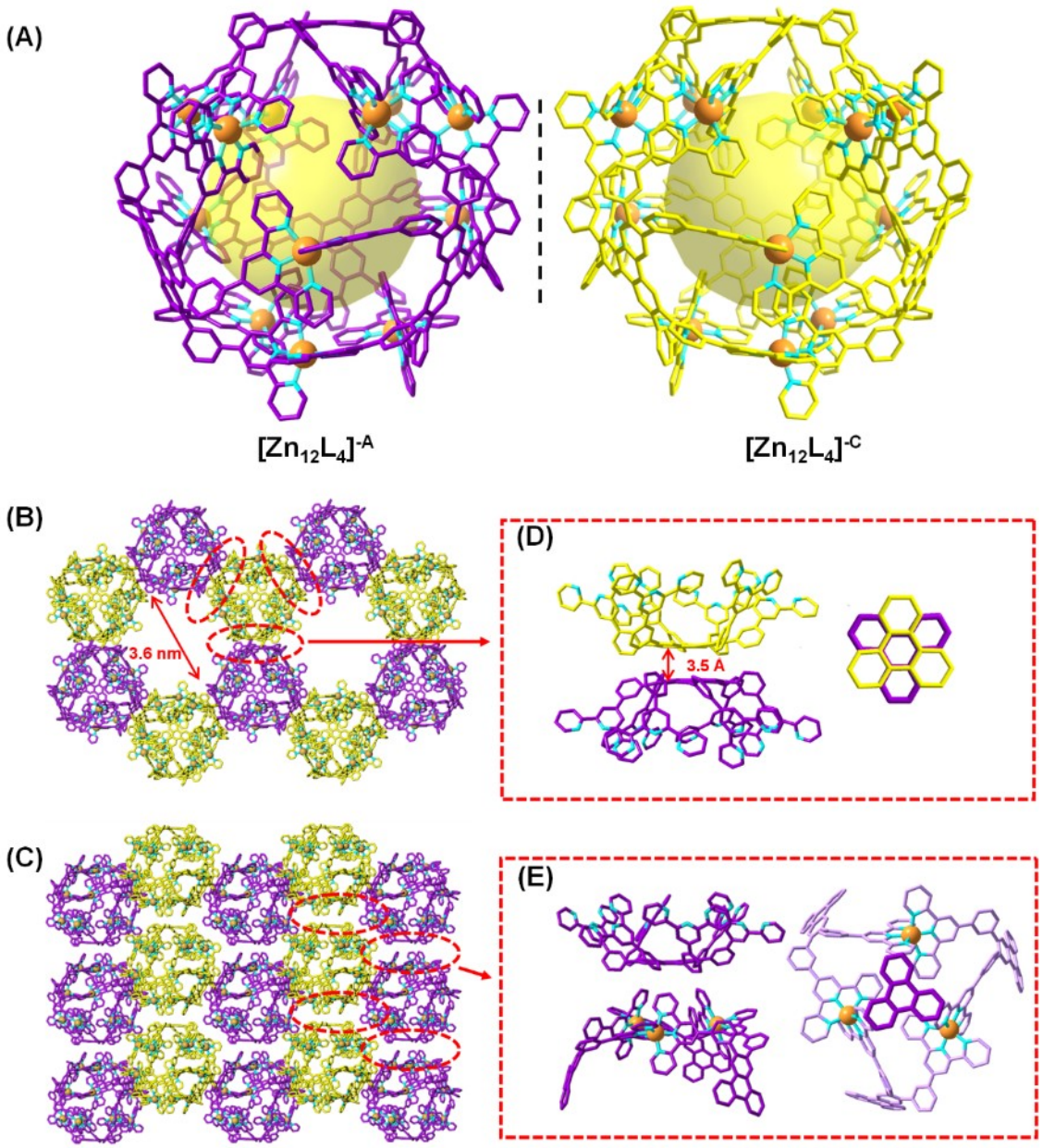

Figure S26. (A) Crystal structure of chiral supramolecular cages $[Zn_{12}L_4]^{-A}$ and $[Zn_{12}L_4]^{-C}$, (B)Top view and (C) front view of the 3D packing for $[Zn_{12}L_4]$, (D) π–π stacking interaction and packing mode between adjacent cages with different chirality, (E) packing mode between adjacent cages with same chirality.

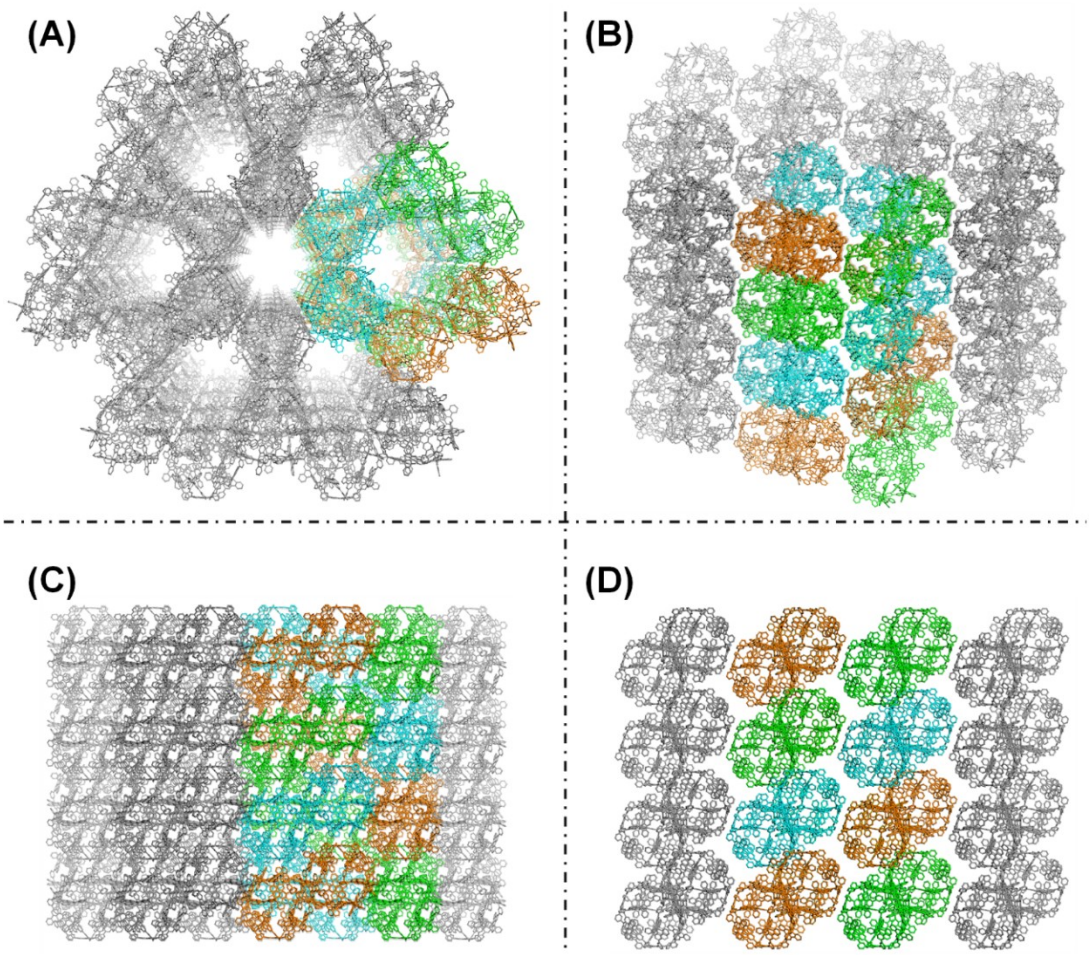

Figure S27. (A) Perspective top view of the "Kagome" topology pattern from the crystal structure. (B,C,D) Crystal structure of **[$Zn_{12}L_4$]** from different view points.

8. Normalized fluorescence spectra and UV-Vis spectra of [$Zn_{12}L_4$]

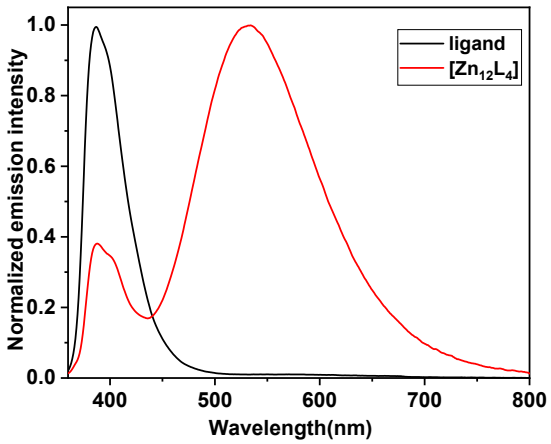

Figure S28. Normalized fluorescence spectra of ligand (in $CHCl_3$) and **[$Zn_{12}L_4$]** (in DMF) (c =1 × 10^{-6} M).

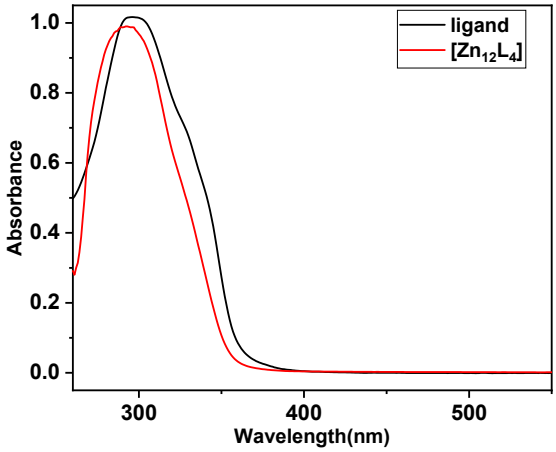

Figure S29. UV-vis of ligand (in $CHCl_3$) and **[$Zn_{12}L_4$]** (in DMF) (c =1 × 10^{-6} M).

9. References

1. Mendecki, L.; Ko, M.; Zhang, X.; Meng, Z.; Mirica, K. A., Porous Scaffolds for Electrochemically Controlled Reversible Capture and Release of Ethylene. *J. Am. Chem. Soc.* **2017,** *139* (48), 17229-17232.

2. Xie, T. Z.; Liao, S. Y.; Guo, K.; Lu, X.; Dong, X.; Huang, M.; Moorefield, C. N.; Cheng, S. Z.; Liu, X.; Wesdemiotis, C.; Newkome, G. R., Construction of a highly symmetric nanosphere via a one-pot reaction of a tristerpyridine ligand with Ru(II). *J. Am. Chem. Soc.* **2014,** *136* (23), 8165-8168.

3. Horcas, I.; Fernandez, R.; Gomez-Rodriguez, J. M.; Colchero, J.; Gomez-Herrero, J.; Baro, A. M., WSXM: a software for scanning probe microscopy and a tool for nanotechnology. *Rev. Sci. Instrum.* **2007,** *78* (1), 013705.